J. COMBIN. MATH. COMBIN. COMPUT. 127b (2025) 2757--2770

Journal of Combinatorial Mathematics and Combinatorial Computing
www.combinatorialpress.com/jcmcc

Research on image segmentation algorithms combining gradient field and variational methods

Yanpin Mei[1,✉]

[1] Yangzhou Polytechnic College, Yangzhou, Jiangsu, 225009, China

ABSTRACT

Image segmentation, as an important direction of computer vision, is gradually being applied to a variety of fields, however, the existing image segmentation methods still need to be improved in terms of segmentation accuracy and effect. In this paper, the variational level set method is used as the level set image segmentation method, and its theoretical basics and solution method (gradient descent flow method) are described in detail. For the problem of insufficient gradient vector flow in the traditional parametric active contour Sanke model, a global gradient vector flow model that can overcome the noise interference is given to obtain a more accurate gradient field, thus combining with the variational level set method to build an image segmentation model based on global gradient vector flow (GGF Snake). In the comparison experiments with three commonly used image segmentation algorithms, the DSC value of this paper's algorithm reaches more than 96.00%, and the time used is less than 15s, which is better than the remaining three algorithms, and verifies the superiority of this paper's algorithm.

Keywords: image segmentation, variational level set method, GGF Snake model, gradient vector flow

1. Introduction

Image segmentation is an important task in computer vision, and its goal is to divide an image into different regions or objects. Image segmentation is widely used in many application fields, such as medical image analysis, target recognition and tracking. Traditional image segmentation methods usually rely on image features such as grayscale, color, and edges for processing, but the results are often not satisfactory in complex scenes. In the past decades, many image segmentation algorithms have been proposed, among which methods based on the variational segmentation method have attracted much attention due to their excellent performance [1-4]. Variational method is a mathematical optimization method which achieves image segmentation by minimizing an energy function. In the image segmentation based on variational method, the image is usually regarded as

✉ Corresponding author.
E-mail address: wind845@163.com (Y. Mei).
Received 30 May 2024; Revised 15 August 2024; Accepted 10 January 2025; Published Online 16 April 2025.
DOI: 10.61091/jcmcc127b-155

the definition domain of an energy function, and the segmentation result is obtained under the minimization of the energy function, and the commonly used energy functions include the full variational difference, Chan-Vese model, etc [5-6].

There are many types and methods of image segmentation, besides the variational method there are gradient fields etc. Some segmentation algorithms can be used directly on any image, while others can only be applied to segment special classes of images. And some algorithms need to coarsely segment the image first, because they need the information extracted from the image. There is no unique standard approach and the good or bad segmentation results need to be measured according to the requirements of the specific occasion [7-8].

Literature [9] explored the problems of image restoration and image segmentation in image processing and pointed out that variational methods can provide optimal solutions when facing these problems, revealing that regularized variational methods are one of the most powerful techniques for solving many image processing tasks. Literature [10] proposes a two-phase selective segmentation method and an image smoothing model, revealing the effectiveness of the method and that the proposed model has attractive mathematical and physical properties to effectively attenuate complex backgrounds while preserving the edges of the target object. Literature [11] proposed an optimization-based multilayer algorithm to efficiently solve a class of selective segmentation models, which is also applicable to the solution of global segmentation models, and the proposed multilayer algorithm has the expected optimal efficiency for images in the level set function formulation. Literature [12] proposed a method combining multiverse optimization approach with variational modal decomposition, which uses the di-entropy function for image segmentation by determining the optimal threshold, revealing that the algorithm is more reliable than the existing algorithms in terms of results. Literature [13] emphasized the excellence of the variational method, and based on the research results of the variational methods for image segmentation, the variational methods were classified into boundary-based models and field-based models, which indicated the development direction of the variational methods for image segmentation. Literature [14] proposes a variational Bayesian based image segmentation method, aiming to demonstrate the framework provided by VB for generalizing existing segmentation algorithms that rely on expectation maximization formulas and increasing their robustness and computational stability. Literature [15] proposed a threshold extraction method based on Variational Modal Decomposition (VMD), indicating that thresholds can be easily extracted by either the Minimum Point Search (MPS) method or the Cross-Point Search (CPS) method, while the MPS scheme provides superior performance over the CPS scheme. Literature [16] proposed a variational level set model for multiscale image segmentation, which can extract the target from the background at different scales, revealing the robustness and effectiveness of the model for multiscale image segmentation, and is a promising model for image denoising. Literature [17] proposed an accurate image segmentation method based on Variational Modal Decomposition (VMD) and Correlation Coefficient (CC) and used K-means method to generate segmentation results, which proved to produce reasonable segmentation results as compared to existing image segmentation methods. Literature [18] investigated the phenomenon of variational methods in image processing that the best image quality can be obtained when the gradient flow process stops before converging to a smooth point and utilized this paradox to introduce the optimal stopping time in the gradient flow process and obtained the optimal stopping time through optimal control methods. The above study discusses the image segmentation of the variational method, and highlights the excellence of this method by comparing it with other segmentation methods, however, also as an image segmentation method, very few scholars have carried out research on the gradient field, and there is no way to talk about the combination of the gradient field and the variational method.

In this paper, the variational level set method is used as the segmentation method for level set images, and the realization principle and process of its segmentation are explained. Subsequently, from the perspective of improving image segmentation accuracy, the basic ideas and numerical algorithms of the classical active contour model (Snake) and GVF Sanke model in image segmentation algorithms are briefly analyzed, as well as the defects in convergence ability. Through the analysis and optimization of the GVF model, a global gradient flow (GGF) model is proposed by combining the variational level set method. Comparison and analysis with similar algorithms and evaluation of image segmentation results based on distributional prior are successively launched to test the effectiveness of the algorithm in this paper.

2. Variational level set methodology

The process of realizing variational level set segmentation of an image is a process of minimizing the energy generalization, and variational method and gradient descent flow are the most commonly used methods to find the extremes of the energy generalization.

2.1. *Principle of variability*

Function $f(x)$ represents a mapping between numbers, with the independent variable being the set of numbers x. Generalized function $E(\phi)$ is a mapping between functions and numbers, with the independent variable being the set of functions $\phi(x)$. In general, the extremum of a function corresponds to the point that makes a first-order derivative $f'(x)=0$, and the extremum of an analogous generalized function corresponds to the function that makes a first-order variable $\frac{\partial E}{\partial \phi}=0$.

For the one-dimensional case, the generalized function is used as in equation (1):

$$E(\phi)=\int_{x_0}^{x_1} F\left(x,\phi,\phi_x\right)dx \tag{1}$$

To find the first-order variant of $E(\phi)$, perturbation of $\phi(x)$ yields $\phi(x)+v(x)$, and when $v(x)$ and $v'(x)$ are sufficiently small, Eq. (2) is obtained from the Taylor expansion:

$$F\left(x,\phi+v,\phi'+v'\right)=F\left(x,\phi,\phi'\right)+\frac{\partial F}{\partial \phi}v+\frac{\partial F}{\partial \phi'}v'+\cdots \tag{2}$$

Thus there is equation (3):

$$E(\phi+v)=E(\phi)+\int_{x_0}^{x_1}\left(\frac{\partial F}{\partial \phi}v+\frac{\partial F}{\partial \phi'}v'\right)dx \tag{3}$$

Equation (4) is obtained based on the fact that the partial integrals and perturbation terms have a value of 0 at the endpoints:

$$\begin{gathered}\int_{x_0}^{x_1} v'\frac{\partial F}{\partial \phi'}dx=\int_{x_0}^{x_i}\frac{\partial F}{\partial \phi'}dv=v\frac{\partial F}{\partial \phi'}\bigg|_{x_0}^{x_i}-\int_{x_0}^{x_i} v\frac{d}{dx}\left(\frac{\partial F}{\partial \phi'}\right)\\ dx=-\int_{x_0}^{x_i} v\frac{d}{dx}\left(\frac{\partial F}{\partial \phi'}\right)dx\end{gathered} \tag{4}$$

Substituting into equation (3) yields equation (5):

$$E(\phi+v)=E(\phi)+\int_{x_0}^{x_1}\left(\frac{\partial F}{\partial \phi}v-v\frac{d}{dx}\left(\frac{\partial F}{\partial \phi'}\right)\right)dx \tag{5}$$

When $E(\phi)$ reaches an extreme value, the value of any sufficiently small perturbation $v(x)$, $E(\phi)$ for $\phi(x)$ remains unchanged, hence Eq. (6):

$$\frac{\partial F}{\partial \phi}-\frac{d}{dx}\left(\frac{\partial F}{\partial \phi'}\right)=0 \tag{6}$$

Equation (6) is called the Euler equation for the variational problem.

For the two-dimensional case equation (7):

$$E(\phi)=\iint_{\Omega} F\left(x, y, \phi, \phi_x, \phi_y\right) dxdy \tag{7}$$

The Euler equation obtained by the same analogy is shown in equation (8):

$$\frac{\partial F}{\partial \phi}-\frac{d}{dx}\left(\frac{\partial F}{\partial \phi_x}\right)-\frac{d}{dy}\left(\frac{\partial F}{\partial \phi_y}\right)=0 \tag{8}$$

After solving the variational components, the problem of solving the energy generalized function extrema is further transformed into solving the corresponding Euler equations. The Euler equations are solved using a gradient descent flow method, which transforms the problem of solving static nonlinear partial differential equations into a dynamic partial differential equation problem by introducing the time variable t, which is iterated continuously in the opposite direction along the gradient to achieve the minimization.

2.2. *Gradient descent flow method*

It is assumed that the required solution varies with time, denoted by $\phi(\cdot,t)$, and that this variation with time always decreases $E(\phi(\cdot,t))$. For the one-dimensional variational case, there is equation (9):

$$E(\phi+v)=E(\phi)+\int_{x_0}^{x_1}\left(\frac{\partial F}{\partial \phi}v-v\frac{d}{dx}\left(\frac{\partial F}{\partial \phi'}\right)\right)dx \tag{9}$$

The minimally used $v(\cdot)$ in Eq. (9) is the amount of change produced by $\phi(\cdot,t)$ from t to $t+\Delta t$, as in Eq. (10):

$$v=\frac{\partial \phi}{\partial t}\Delta t \tag{10}$$

Equation (9) can then be rewritten as equation (11):

$$E(\cdot,t+\Delta t)=E(\cdot,t)+\Delta t\int_{x_0}^{x_1}\frac{\partial \phi}{\partial t}\left(\frac{\partial F}{\partial \phi}-\frac{d}{dx}\left(\frac{\partial F}{\partial \phi'}\right)\right)dx \tag{11}$$

It is only necessary to make Eq. (12):

$$\frac{\partial \phi}{\partial t}=-\left[\frac{\partial F}{\partial \phi}-\frac{d}{dx}\left(\frac{\partial F}{\partial \phi'}\right)\right]=\frac{d}{dx}\left(\frac{\partial F}{\partial \phi'}\right)-\frac{\partial F}{\partial \phi} \tag{12}$$

It is then possible to make $E(\phi(\cdot,t))$ continuously decreasing, which is then called Equation (13):

$$\frac{\partial \phi}{\partial t}=\frac{d}{dx}\left(\frac{\partial F}{\partial \phi'}\right)-\frac{\partial F}{\partial \phi} \tag{13}$$

is equation (14):

$$E(\phi)=\int_{x_0}^{x_1} F\left(x, \phi, \phi_x\right) dx \tag{14}$$

corresponding gradient descent flow.

For the two-dimensional variational case, the gradient descent flow is similarly obtained as Eq. (15):

$$\frac{\partial \phi}{\partial t}=\frac{d}{dx}\left(\frac{\partial F}{\partial \phi_x}\right)+\frac{d}{dy}\left(\frac{\partial F}{\partial \phi_y}\right)-\frac{\partial F}{\partial \phi} \tag{15}$$

An initial level set function ϕ_0 is chosen to be computed iteratively according to the gradient descent flow until a stable solution is obtained, and the zero level set of the level set function at this point is taken as the segmentation result.

3. Image segmentation model based on global gradient flow

The goal of image segmentation is to divide the target region from the background region based on various image feature elements, or to divide the image into several regions that do not overlap each other. In this chapter, an image segmentation model for global gradient flow (GGF Snake) is proposed on the basis of Sanke's segmentation model, combined with the variational level set method above.

3.1. Snake Model

An active contour model based on edge information was first proposed in 1988. Since the model contains parametric information, the model is also known as the parametric active contour model. This model is the classical edge-based active contour model, and a large number of improved models have emerged since then based on this model. First, an initialized closed curve containing parameters is defined as in equation (16):

$$c(q)=[x(q),y(q)],\, q\in[0,1] \tag{16}$$

Next the energy function is constructed see equation (17). By minimizing the following energy generalization, the initialization curve evolves towards the target edge under the internal force of its own curve as well as the external force constituted by the image information:

$$E(c(q))=\underbrace{\frac{1}{2}\int_0^1 \alpha\,|\,c(q)\,|^2+\beta\,|\,c(q)\,|^2\,dq}_{\text{internal energy}}+\underbrace{\int_0^1 E_{ev}(c(q))dq}_{\text{external energy}} \tag{17}$$

where the energy function consists of the internal energy of the curve itself and the external energy consisting of image information. The internal energy of the curve in the first term takes into account the geometry of the contour and imposes smoothness constraints on the contour so that the contour curve stretches and bends. In the first term of the first-order differential, the physical meaning of the second-order differential is the continuity of the contour curve and the curvature of each point, and α,β is the weighting coefficient. α represents the tension coefficient, which controls the contraction amplitude of the contour curve, and the tension coefficient is proportional to the contraction speed of the curve. β is the stiffness coefficient, which controls the speed of movement of the contour curve along the normal direction toward the target boundary. The second term is the external energy term, which contains information about the data in the image and is related to the image features.

The process of minimizing Eq. (17) by iteration is the process of driving the contour curve towards the edge of the target contour under the combined effect of internal and external energies. According to the variational method, the curve must satisfy the Euler-Lagrange equation as in Eq. (18):

$$\frac{\partial}{\partial q}\left(\alpha\frac{\partial c}{\partial q}\right)-\frac{\partial^2}{\partial q^2}\left(\beta\frac{\partial^2 c}{\partial q^2}\right)-\nabla\varepsilon_{external}(c(q))=0 \tag{18}$$

where $\nabla\varepsilon_{external}$ is the Gaussian external force field, and this parametric activity model based on Gaussian external forces is also known as the snake model. In order to solve Eq. (18), the model can be converted into a dynamic activity model by introducing the time parameter t and considering the curve $c(q)$ as a dynamic function $c(q,t)$ of time t. Eq. (18) is transformed into Eq. (19):

$$\frac{\partial c}{\partial t}=\frac{\partial}{\partial q}\left(\alpha\frac{\partial c}{\partial q}\right)-\frac{\partial^2}{\partial q^2}\left(\beta\frac{\partial^2 c}{\partial q^2}\right)-\nabla\varepsilon_{extenal}(c(q))=0 \tag{19}$$

3.2. *Global Gradient Flow Model (GGF)*

In response to the classical Snake model's lack of dependence on the initial contour line and the ability of the external force to converge to the depressed region, the GVFSnake model compensates for this by using external forces that do not depend on the position of the initial curve contour. However, the GVF model still suffers from the problem of having a limit on the ability to converge to deep recessed regions. If the concave region becomes very narrow, the GVF Snake model still cannot converge to the boundary of the target. For this reason, this section proposes the global gradient flow (GGF) model as in equation (20):

$$\begin{aligned}E=&\frac{1}{|\Omega|}\iint_{\Omega\times\Omega}\omega_{xy}^{s}(f(x)-f(y)+V(x)\cdot(y-x))^2\,dydx\\&+\lambda\|\nabla V\|_{L^2}^2\end{aligned} \tag{20}$$

where λ is the parameter. When $\|\nabla V\|_{L^2}^2=u_1^2+u_2^2+v_1^2+v_2^2$. Here the weight function is defined as equation (21):

$$\omega_{xy}^{s}=|\nabla f(x)|^2\exp\left(-\frac{|y-x|^2}{S^2}\right) \tag{21}$$

The size of the weight function ω_{xy}^{s} is related not only to the distance between two points x and y, but also to $|\nabla f(x)|$. When ∇f takes a large value and point x is located on (or near) the boundary, the first term in Eq. (22) plays a key role in estimating the gradient of point x more accurately by using the information from the surrounding points. When $|\nabla f|$ takes a very small value and point x is far away from the boundary, the second term in Eq. (22) plays a major role by making V the vector field at the edges spread out to the surroundings, allowing the vector field V to change more smoothly. In addition, when the image contains noise or the background is complex, the first term is utilized to suppress the interference of noise and find the main edges.

Similar to the GVFSnake model, the GGFSnake model first uses the GGF to find the vector field V^* and then brings it into the computational formula to get Eqs. (22), (23):

$$\begin{aligned}&V^*=\arg\min_{V}\\&\left\{\frac{1}{|\Omega|}\iint_{\Omega\times\Omega}\omega_{xy}^{s}(f(x)-f(y)+V(x)\cdot(y-x))^2\,dydx+\lambda\|\nabla V\|_{L^2}^2\right\}\end{aligned} \tag{22}$$

$$C_t(x)=\alpha C''(x)+\beta C''''(x)+V^* \tag{23}$$

3.3. *Implementation of the GGF Snake model*

To solve Eq. (22), the Euler equations of the model are first given as Eq. (24):

$$0=\lambda div(\nabla V(x))-\frac{2}{|\Omega|}\int_{\Omega}\omega_{xy}^{s}(f(x)-f(y)+V(x)\cdot(y-x))(y-x)dy \tag{24}$$

The evolution equation can then be obtained as Eq. (25):

$$\frac{\partial V(x,t)}{\partial t}=\lambda div(\nabla V(x,t)).-\frac{2}{|\Omega|}\int_{\Omega}\omega_{xy}^{s}(f(x)-f(y)+V(x,t)\cdot(y-x))(y-x)dy \tag{25}$$

The discrete format of Eq. (25) is then obtained as Eq. (26) using the explicit Euler formula:

$$\frac{V_i^{k+1}-V_i^k}{\tau_2}=\frac{1}{\Delta_1\Delta_2}\left(V_{i+1,j}^n+V_{i,j+1}^n+V_{i-1,j}^n+V_{i,j-1}^n-4V_{i,j}^n\right)-\frac{2}{\left|\mathrm{N}_i\right|}\sum_{y\in \mathrm{N}_i}\omega_{ij}^{s}\left(f_i-f_j+V_i^k\cdot\left(x_j-x_i\right)\right)\left(x_j-x_i\right)^T \tag{26}$$

where i, j, and n correspond to variables x_1, x_2, and t, respectively, with spatial steps of Δ_1, Δ_2, and time steps of Δt. $V_i^k=\left(u_i^k,v_i^k\right)$, $x_i=\left(i\Delta_1,i\Delta_2\right)$.

4. Application and analysis of the GGF Sanke model

Comparing similar algorithms and evaluating segmentation results based on distributional priors is an effective way to test the performance of image segmentation models. In this chapter, the selection of the fractional order differential order of the model is firstly developed as the basis for numerical experiments of the model. Then the comparison between the model algorithm of this paper and three commonly used algorithms is developed, and finally the image segmentation results based on distributional prior of the model of this paper are evaluated.

4.1. Selection of the fractional order of differentiation

Fractional order differentiation can act on the narrowband neighborhood of each pixel in the image with arbitrary bandwidth, thus considering more neighborhood pixel features. The problem of selecting the differential order in the fractional order edge detection operator is analyzed below from the perspective of frequency characteristics. The amplitude-frequency characteristic response curves for several typical orders at differential order α ∈ [0,2.0] are given in Fig. 1.

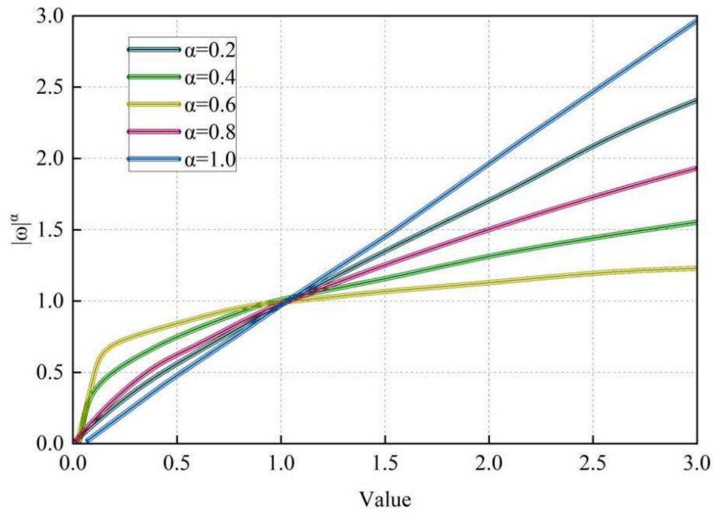

(a) α∈(0,1.0]

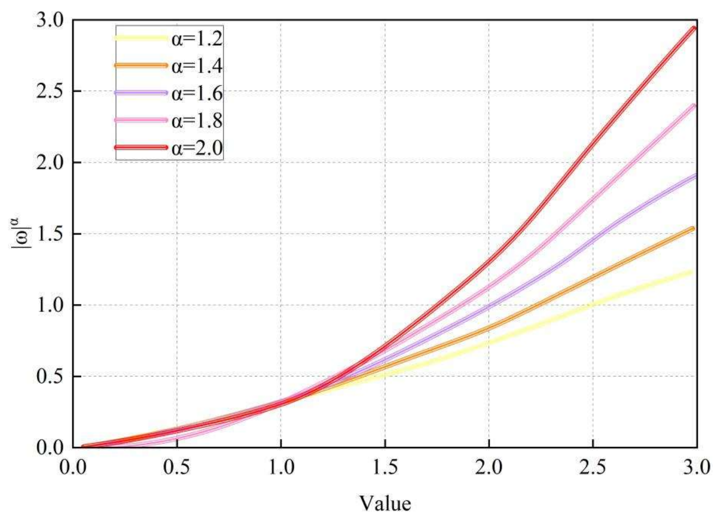

(b) α∈(1.0,2.0]

Fig. 1. Amplitude-frequency response

It is clear that when $\alpha \in (0,1.0]$, in the very low frequency part, which corresponds to the smooth region of the image, fractional order differencing enhances the contour characteristics of the image nonlinearly compared to first order differencing. In the mid-frequency part, which corresponds to the texture region of the image, fractional order differencing preserves the detail characteristics of the image compared to the first order differencing, while in the high frequency part, which corresponds to the edges and the noise components of the image, fractional order differencing has a significant reduction effect compared to the first order differencing. And when $\alpha \in (1.0,2.0]$, the amplitude-frequency characteristic curve shows a rapid nonlinear growth trend with the increase of frequency and differential order. In the very low-frequency part, fractional-order differentiation and first-order differentiation have similar weakening effects on the whorl features in the smooth region of the image. However, in the high-frequency part, the fractional-order differentiation is significantly better than the first-order differentiation in enhancing the high-frequency noise and edge information of the image.

Taking into account the feature retention ability of edge detection for smooth and textured regions and the robustness to noise, the fractional order $\alpha \in (0,1.0]$ is selected in this paper for extracting more detailed information about the image edges.

4.2. Comparison experiments with similar algorithms

This subsection unfolds the performance comparison between the model algorithm of this paper and three similar algorithms commonly used LHDCMG, CCZ, and Cai for segmenting images, specifically comparing the image segmentation performance, and evaluation of segmentation result indexes.

4.2.1. Image Segmentation Performance. In the first experiment, a CT liver image A was selected as the original image. Figures A(A1)-(A2) represent the original image and the image with noise, respectively. Figure A(A3) shows the blurred image obtained by acting on the original image with a Gaussian kernel of size 15*15 and standard deviation 15. Fig. A(A4) shows the blurred image with motion kernel (15 pixels and angle 90°).

The purpose of the second experiment is to test whether the model in this paper can handle blurred images well and compare it with LHDCMG, CCZ, and Cai models. In this paper, the two most popular Gaussian kernel and motion kernel are selected to de-blur the image to get image B. Figure B (b) is blurred by Gaussian kernel with size 15*15 and standard deviation 15, (g) is blurred by motion kernel (15 pixels and angle 90°), (1) is blurred by Gaussian kernel (size 15*15 and standard deviation 3) , (q) blurred by motion kernel (15 pixels and angle 45°).

Table 1 shows the comparison experimental results of the commonly used algorithms LHDCMG, CCZ, Cai and the model algorithm of this paper. It can be seen that in the processing of image A, this paper's algorithm can achieve good segmentation results, the time used is shorter, are below 1.0s, and can achieve the highest DC with fewer iterations. in the processing of image B, CCZ algorithm and this paper's algorithm for selecting different fuzzy kernels are able to achieve good experimental results. However, the number of iterations and the time used by this paper's algorithm are still at the top of the list, i.e., this paper's model can distinguish more details in a short period of time.

Table 1. Iteration steps and CPU time (seconds)

		Figure A				Figure B			
		A1	A2	A3	A4	B1	B2	B3	B4
LHDCMG	iteration	1200	4800	1800	500	50	50	50	50
	time	162.84	698.81	239.16	19.99	10.98	10.78	10.72	10.98
CCZ	Iteration	6	6	9	14	7	8	9	9
	Time	0.82	0.83	2.31	2.35	0.48	0.52	0.54	0.49
Cai	Iteration	7	16	6	6	25	25	25	25
	Time	1.42	2.82	1.37	1.39	2.01	1.83	1.82	1.77
GGF Snake	Iteration	6	5	6	6	3	3	3	3
	Time	0.67	0.60	0.69	0.74	0.45	0.49	0.49	0.50

The parameter settings of the commonly used algorithms LHDCMG, CCZ, Cai and the model algorithm of this paper for processing image A in the comparison test are shown in Table 2.

Table 2. Compare the parameter Settings of the two algorithms in the experiment

Figure A		A1	A2	A3	A4
LHDCMG	λ	$0.06*255^2$	$0.02*255^2$	$0.04*255^2$	$0.05*255^2$
	μ	0.003	0.002	0.2	0.06
CCZ	λ	3	2	100	100
	μ	2	6	4	2
Cai	λ	5	11	25	6
	μ	100*λ	100*λ	100*λ	100*λ
GGF Snake	λ	100	23	150	150
	μ	2000*λ	3000*λ	2000*λ	2000*λ

4.2.2. Assessment of Segmentation Outcome Indicators. Table 3 shows the DSC value, HD value, number of convergence iteration steps and convergence time of different algorithms in segmenting graph A. The DSC value is the Dice similarity coefficient. The DSC value is the Dice similarity coefficient, and the HD value is the Hausdorff distance, both of which are quantitative evaluation indexes of the segmentation accuracy of different algorithms. In this paper, when the algorithm segments the graph A, the DSC value reaches more than 95.00%, the corresponding HD value is the lowest among the four algorithms, which is below 1.800, and the number of iterative convergence steps is also the smallest among the four algorithms, which is between 0-50 steps, and the time used is only less than 10s, which indicates that this paper's algorithm not only converges fast, but also segments the segmentation with higher accuracy.

Table 3. Figure A segmentation results performance of different algorithms

Figure A	evaluation index	LHDCMG	CCZ	Cai	GGF Snake
A1	DSC	77.79%	92.49%	92.63%	96.37%
	HD	3.8191	2.2156	1.701	1.2661
	Iter	25	485	601	25
	Time	112.32	73.01	88.86	7.78
A2	DSC	76.99%	85.63%	93.04%	95.41%
	HD	4.2859	3.1260	2.1252	1.7917
	Iter	385	500	4785	39
	Time	107.58	74.87	78.47	12.17
A3	DSC	74.96%	86.42%	92.88%	95.92%
	HD	3.7833	2.7438	1.8524	1.6729
	Iter	385	505	625	35
	Time	106.15	84.64	89.46	10.04
A4	DSC	75.23%	84.95%	90.61%	96.63%
	HD	3.5621	2.5361	1.7436	1.7216
	Iter	350	520	410	30
	Time	100.21	80.21	85.37	9.63

Table 4 shows the DSC value, HD value, convergence iteration step, and convergence time of different algorithms in segmentation plot B. When dividing graph B, the DSC value of the proposed algorithm is more than 96.00%, the corresponding HD value is the lowest among the four algorithms, below 1.200, and the number of iterative convergence steps is also the least among the four algorithms, all between 0 and 50 steps, and the time taken is only less than 15s, indicating that compared with the LHDCMG algorithm, CCZ algorithm and Cai algorithm, the proposed algorithm achieves the best segmentation effect, and its convergence time and iteration steps are also significantly better than those of other algorithms.

Table 4. Figure B segmentation results performance of different algorithms

Figure B	evaluation index	LHDCMG	CCZ	Cai	GGF Snake
B1	DSC	88.93%	93.98%	96.44%	96.44%
	HD	0.9941	2.2063	1.1992	1.0871
	Iter	185	720	320	37
	Time	45.41	107.63	45.23	13.22
B2	DSC	88.68%	93.55%	96.34%	96.39%
	HD	1.0918	2.0745	1.1474	1.1337
	Iter	335	855	455	35
	Time	97.95	121.28	62.45	9.14
B3	DSC	88.29%	92.54%	96.38%	96.44%
	HD	1.2311	2.5351	1.1747	1.0991
	Iter	600	905	279	40
	Time	153.87	126.68	43.08	11.42
B4	DSC	88.30%	91.14%	95.24%	96.78%
	HD	1.3467	2.3416	1.2458	1.1436
	Iter	610	962	274	36
	Time	163.24	117.61	45.69	12.36

4.3. Segmentation results based on distributional prior

Distribution of prior information can effectively improve the segmentation effect and segmentation effect, based on this, this subsection uses the algorithm of this paper to segment the synthetic images C and D with different noises added to verify the effectiveness of the algorithm of this paper.

Image C is a synthetic image with noise, Figure 2 shows the corresponding contour curve and probability density distribution of this paper's model on synthetic image C. Where Fig. 2(a)-(e) are the a priori contour, contour initialization, pre-segmentation process, post-segmentation process, and final segmentation result of this image, respectively. By observing Fig. 2(a) and Fig. 2(e), it can be found that the a priori contour and the final segmentation result are not different, i.e., the model in this paper can effectively segment the image.

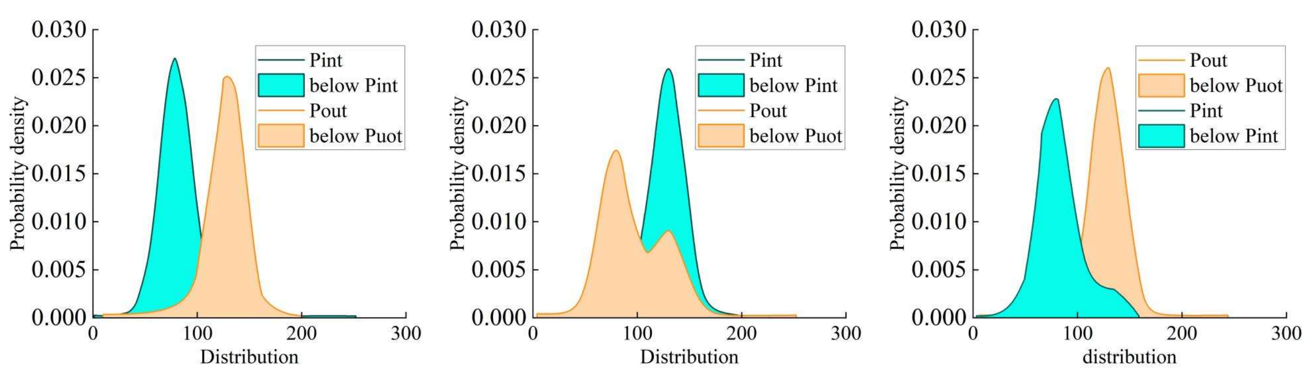

(a) Prior contour (b) Contour initialization (c) Prephase of segmentation

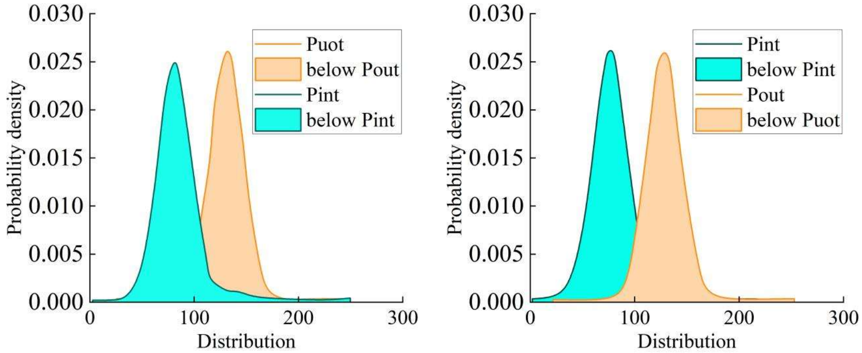

(d) Late partition (e) Final segmentation result

Fig. 2. The segmentation process of Figure C by the algorithm in this paper

Figure D shows an aerial photograph of an airplane whose target is a parked airplane, and Figure 3 shows the corresponding probability density distribution of this paper's model over the synthetic image D. Its a priori image is a black and white photograph of an airplane. It is worth noting that the a priori contours in the a priori image are roughly selected by hand and are not strictly the contours of the aircraft, this is because the algorithm needs the a priori statistical information of the aircraft and the specific contours of the a priori aircraft are not important. Comparing the contour models in Fig. 3(a) and Fig. 3(e), the overall contour Pint of the a priori airplane is no different from the final segmentation result, which verifies the superior performance of this paper's algorithm in segmenting images.

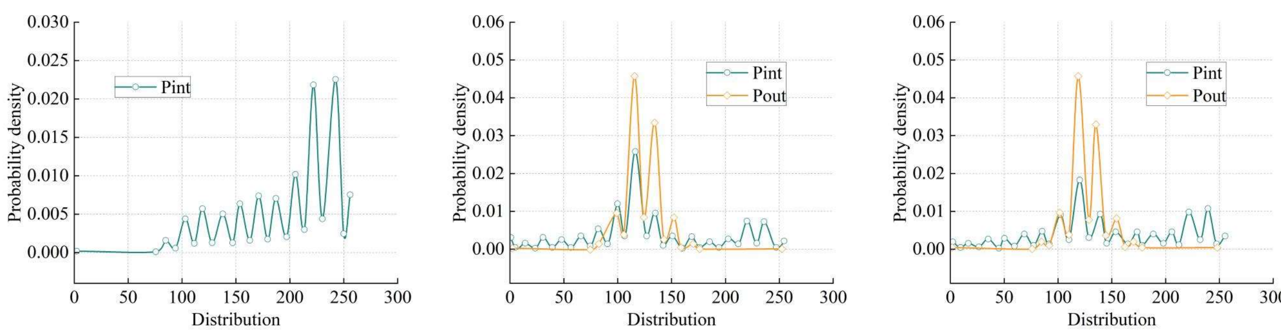

(a) Prior contour (b) Contour initialization (c) Prephase of segmentation

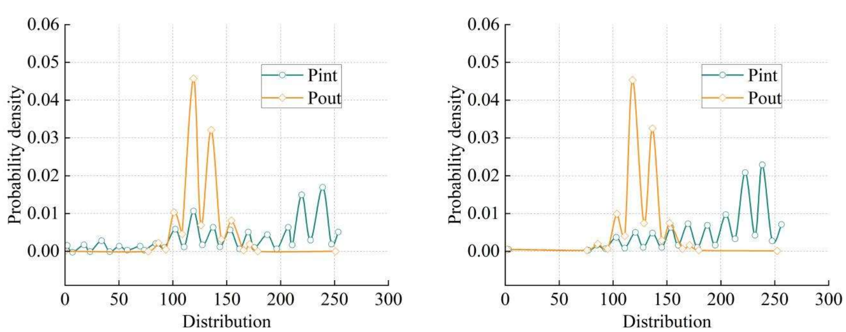

(d) Late partition (e) Final segmentation result

Fig. 3. The segmentation process of Figure D by the algorithm in this paper

5. Conclusion

In this paper, a new image segmentation method is proposed by using the variational level set method as the energy generalized function to find the extreme value, and optimizing the traditional Snake image segmentation model in order to build an image segmentation model based on the global gradient flow.

In the comparison experiments with similar algorithms, the DSC values of this paper's algorithm are all above 96.00%, and the time used is less than 15s. In the segmentation experiments based on distributional prior, the final results of the segmentation of artificial images by this paper's algorithm are consistent with the prior contour. That is, compared with other algorithms, the GGF snake model can converge well to the boundary of the deep concave region and has the advantage of good resistance to noise interference.

Funding

This research was supported by the 2023 University-level key research project: 2023 "Qinglan Project" of Jiangsu Universities.

References

[1] Minaee, S., Boykov, Y., Porikli, F., Plaza, A., Kehtarnavaz, N., & Terzopoulos, D. (2021). Image segmentation using deep learning: A survey. IEEE transactions on pattern analysis and machine intelligence, 44(7), 3523-3542.

[2] Yu, Y., Wang, C., Fu, Q., Kou, R., Huang, F., Yang, B., ... & Gao, M. (2023). Techniques and challenges of image segmentation: A review. Electronics, 12(5), 1199.

[3] Liu, X., Deng, Z., & Yang, Y. (2019). Recent progress in semantic image segmentation. Artificial Intelligence Review, 52, 1089-1106.

[4] Ramesh, K. K. D., Kumar, G. K., Swapna, K., Datta, D., & Rajest, S. S. (2021). A review of medical image segmentation algorithms. EAI Endorsed Transactions on Pervasive Health and Technology, 7(27), e6-e6.

[5] Bauer, B., Cai, X., Peth, S., Schladitz, K., & Steidl, G. (2017). Variational-based segmentation of bio-pores in tomographic images. Computers & Geosciences, 98, 1-8.

[6] Jin, Z., Wu, Y., Min, L., & Ng, M. K. (2020). A Retinex-based total variation approach for image segmentation and bias correction. Applied Mathematical Modelling, 79, 52-67.

[7] Anjna, E., & Kaur, E. R. (2017). Review of image segmentation technique. International Journal of Advanced Research in Computer Science, 8(4), 36-39.

[8] Abdulateef, S. K., & Salman, M. D. (2021). A Comprehensive Review of Image Segmentation Techniques. Iraqi Journal for Electrical & Electronic Engineering, 17(2).

[9] Vese, L. A., & Le Guyader, C. (2016). Variational methods in image processing. Boca Raton: CRC Press.

[10] Zhao, W., Wang, W., Feng, X., & Han, Y. (2022). A new variational method for selective segmentation of medical images. Signal Processing, 190, 108292.

[11] Chen, K., & Jumaat, A. (2017). An optimization based multilevel algorithm for variational image segmentation models. Electronic Transactions on Numerical Analysis, 46, 474-504.

[12] Chouksey, M., & Jha, R. K. (2021). A multiverse optimization based colour image segmentation using variational mode decomposition. Expert Systems with Applications, 171, 114587.

[13] Tian, Y., & Xue, Y. (2020, March). Variation method overview of image segmentation. In Journal of Physics: Conference Series (Vol. 1487, No. 1, p. 012012). IOP Publishing.

[14] Blaiotta, C., Cardoso, M. J., & Ashburner, J. (2016). Variational inference for medical image segmentation. Computer Vision and Image Understanding, 151, 14-28.

[15] Li, J., Tang, W., Wang, J., & Zhang, X. (2018). Multilevel thresholding selection based on variational mode decomposition for image segmentation. Signal Processing, 147, 80-91.

[16] Zhang, H., Tang, L., & He, C. (2019). A variational level set model for multiscale image segmentation. Information Sciences, 493, 152-175.

[17] Hao, D., Li, Q., & Li, C. (2017). Histogram-based image segmentation using variational mode decomposition and correlation coefficients. Signal, Image and Video Processing, 11, 1411-1418.

[18] Effland, A., Kobler, E., Kunisch, K., & Pock, T. (2020). Variational networks: An optimal control approach to early stopping variational methods for image restoration. Journal of mathematical imaging and vision, 62, 396-416.